

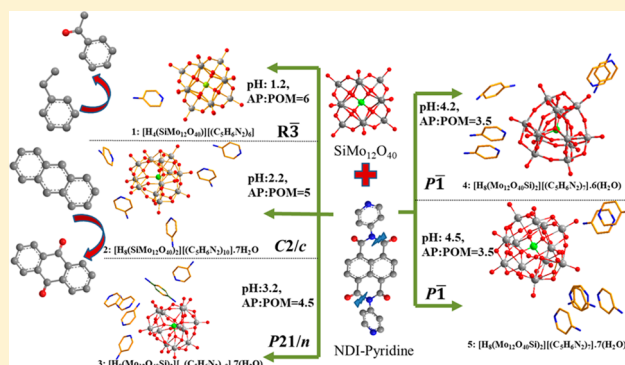
Crystal Engineering in Supramolecular Polyoxometalate Hybrids through pH Controlled in Situ Ligand Hydrolysis

Soumyabrata Roy, Dundappa Mumbaraddi,¹ Ankit Jain, Subi J. George,² and Sebastian C. Peter^{*,1}

New Chemistry Unit, Jawaharlal Nehru Centre for Advanced Scientific Research, Jakkur, Bangalore, 560064, India

S Supporting Information

ABSTRACT: A family of five different three-dimensional polyoxometalate (POM) based supramolecular hybrids were synthesized by a hydrothermal route under different pH using a hydrolyzable naphthalene diimide ligand. The mechanism of crystallographic phase variation of the POM-amino pyridine hybrids under different pH was studied through controlled experiments where the final hydrolyzed products were analyzed through NMR and single crystal X-ray diffraction. Different pH conditions led to variation in the extent of protonation and hydrolyzation of the ligand, yielding different phases. All of these were identified, and the structures of the supramolecular hybrids were characterized extensively. Mechanistic study proved that only the reaction conditions are responsible for the hydrolysis of the ligand and the in situ generated POM species do not have any role in it. Magnetic measurements confirmed the hexavalent oxidation states of the transition metal center (Mo) in the POM. Optical band gap measurements revealed that these hybrids are semiconducting in nature. Two of the compounds were studied for hydrogen peroxide mediated selective oxidation catalysis of small organic molecules and found to exhibit very good activity with high percentage of selectivity for the desired products of industrial importance.



1. INTRODUCTION

Polyoxometalates (POMs), a class of oxy-anion clusters of early transition metals (TM = Cr, V, Mo, W, Nb) in the highest oxidation states, are well-known for their extensive applications in fields ranging from materials to biological sciences.^{1–6} The properties of POMs, originating from the rich redox chemistry of transition metals, anionic nature of oxygen centers, and hydrolyzable protons, have found immense applications in catalysis (chemical, photochemical, electrochemical), single molecule magnets, molecular electronics, optical properties, medicinal chemistry, biology, and bioinorganic synthesis.^{5–12} The sensitivity of POMs-hybrid structural hierarchy toward reaction conditions like pH, temperature, and reaction time is often used as an important tool to modulate the structure and properties of this class of compounds. The structure and electrochemical properties of the POMs also exhibit a strong dependence on pH.^{13–15} pH governs the extent of protonation and hence basicity of the organic ligands, which eventually determines the dimensional complexity and nature of interactions in these hybrids.^{16–19} The dimensionality of POM based hybrids can be increased by coordinating properties of the organic ligands involved and incorporation of secondary transition metals, which enhances the catalytic, optical, and electronic properties of the POMs. The nitrogen containing ligands with donor properties often act as directing agents in the hybrids and determine the dimensionality of the structures.²⁰ These nitrogen donor centers can also reduce Mo or TM of the

POMs to form mixed valent systems with enhanced electronic properties. In the absence of secondary TMs, the ligands tend to form supramolecular hybrids having direct, noncovalent interactions with their inorganic counterparts. The electron donating capacity of the nitrogen centers can be tuned by variation of H⁺ ion concentration in the system, which gives a fine control over the dimensionality, structural interactions, and crystal phase engineering of the system. However, due to lack of control over protonation of the ligands, mixed phases and isomorphs are common problems in such supramolecular assemblies. An innovative way to solve the issue is to incorporate the ligand into a hydrolyzable precursor form, which may give controlled release and protonation of the coordinating ligand. A simple reaction condition like pH can be used to engineer the crystallographic phase of such systems, the mechanistic investigation of which may give valuable insights into the dynamic role of the reaction conditions.

Here, we report five supramolecular 3D hybrid compounds (1, 2, 3, 4, and 5) comprising Keggin POM (SiMo₁₂O₄₀⁴⁻) and 4-amino pyridine (4-ap) that have been synthesized under hydrothermal reaction conditions by in situ POM formation and hydrolysis of a pyridyl naphthalene diimide (NDI-py) ligand. pH triggered NDI-py hydrolysis yielded a controlled amount of the reacting ligand, 4-ap, under the reaction conditions. We have

Received: September 16, 2017

Table 1. Crystal Data and Structure Refinement Parameters for 1 $[\text{H}_8(\text{SiMo}_{12}\text{O}_{40})_2][(\text{C}_5\text{H}_6\text{N}_2)_{10}] \cdot 7\text{H}_2\text{O}$, **2** $[\text{H}_4(\text{SiMo}_{12}\text{O}_{40})][(\text{C}_5\text{H}_6\text{N}_2)_6]$, **3** $[\text{H}_8(\text{Mo}_{12}\text{O}_{40}\text{Si})_2][(\text{C}_5\text{H}_6\text{N}_2)_9] \cdot 7(\text{H}_2\text{O})$, **4** $[\text{H}_8(\text{Mo}_{12}\text{O}_{40}\text{Si})_2][(\text{C}_5\text{H}_6\text{N}_2)_7] \cdot 6(\text{H}_2\text{O})$, and **5** $[\text{H}_8(\text{Mo}_{12}\text{O}_{40}\text{Si})_2][(\text{C}_5\text{H}_6\text{N}_2)_7] \cdot 7(\text{H}_2\text{O})^a$

	1	2	3	4	5
empirical formula	$\text{C}_{30}\text{H}_{36}\text{Mo}_{12}\text{N}_{12}\text{O}_{40}\text{Si}$	$\text{C}_{50}\text{H}_{67}\text{Mo}_{24}\text{N}_{20}\text{O}_{87}\text{Si}_2$	$\text{C}_{45}\text{H}_{58}\text{Mo}_{24}\text{N}_{18}\text{O}_{87}\text{Si}_2$	$\text{C}_{35}\text{H}_{54}\text{Mo}_{24}\text{N}_{14}\text{O}_{86}\text{Si}_2$	$\text{C}_{35}\text{H}_{50}\text{Mo}_{24}\text{N}_{14}\text{O}_{87.61}\text{Si}_2$
formula weight	2384.08	4663.69	4601.83	4405.66	4427.32
temperature	298 K	296.45 K	100.0 K	100.0 K	293 K
wavelength	0.71073 Å	0.71073 Å	0.71073 Å	0.71073 Å	0.71073 Å
crystal system	rhombohedral	monoclinic	monoclinic	triclinic	triclinic
space group, Z	$R\bar{3}, 3$	$C2/c, 4$	$P2_1/n, 2$	$P\bar{1}, 1$	$P\bar{1}, 1$
unit cell dimensions	$a = 21.8664(3)$ Å $b = 21.8664(3)$ Å $c = 10.5150(2)$ Å	$a = 42.1438(19)$ Å $b = 12.2492(5)$ Å $c = 25.2517(10)$ Å $\beta = 115.802(3)^\circ$	$a = 21.2231(13)$ Å $b = 12.3452(7)$ Å $c = 22.9950(14)$ Å $\beta = 113.160(2)^\circ$	$a = 10.4802(7)$ Å $b = 11.7748(8)$ Å $c = 21.0804(15)$ Å $\alpha = 75.265(4)^\circ$ $\beta = 77.340(3)^\circ$ $\gamma = 86.720(4)^\circ$	$a = 11.3922(5)$ Å $b = 15.1799(6)$ Å $c = 15.9743(7)$ Å $\alpha = 91.188(2)^\circ$ $\beta = 107.447(2)^\circ$ $\gamma = 100.744(2)^\circ$
volume	$4354.06(15)$ Å ³	$11736.0(9)$ Å ³	$5539.2(6)$ Å ³	$2454.6(3)$ Å ³	$2580.52(19)$ Å ³
density (calcd)	2.728 g/cm ³	2.639 g/cm ³	2.759 g/cm ³	2.980 g/cm ³	2.849 g/cm ³
absorption coefficient	2.633 mm ⁻¹	2.605 mm ⁻¹	2.757 mm ⁻¹	3.101 mm ⁻¹	2.952 mm ⁻¹
$F(000)$	3414	8816	4372	2086	2095
crystal size	$0.15 \times 0.1 \times 0.04$ mm ³	$0.12 \times 0.08 \times 0.02$ mm ³	$0.14 \times 0.06 \times 0.04$ mm ³	$0.12 \times 0.04 \times 0.02$ mm ³	$0.200 \times 0.120 \times 0.040$ mm ³
θ range for data collection	$2.895\text{--}25.597^\circ$	$2.215\text{--}29.200^\circ$	$2.215\text{--}26.466^\circ$	$2.270\text{--}25.000^\circ$	$2.551\text{--}24.999^\circ$
index ranges	$-26 \leq h \leq 26$ $-26 \leq k \leq 19$ $-12 \leq l \leq 12$	$-57 \leq h \leq 57$ $-16 \leq k \leq 16$ $-34 \leq l \leq 34$	$-26 \leq h \leq 26$ $-15 \leq k \leq 15$ $-28 \leq l \leq 28$	$-12 \leq h \leq 12$ $-13 \leq k \leq 13$ $-25 \leq l \leq 25$	$-13 \leq h \leq 13$ $-18 \leq k \leq 18$ $-18 \leq l \leq 18$
reflins collected	23764	261901	122765	46777	89245
independent reflins	1812 [$R_{\text{int}} = 0.0557$]	15870 [$R_{\text{int}} = 0.0389$]	11387 [$R_{\text{int}} = 0.0736$]	8573 [$R_{\text{int}} = 0.0941$]	9028 [$R_{\text{int}} = 0.0336$]
completeness to $\theta = 26.000^\circ$	99.8%	99.8%	99.9%	99.3%	99.3%
data/restraints/parameters	1812/0/150	15870/0/807	11387/0/811	8573/43/761	9028/72/810
refinement method	full-matrix least-squares on F^2				
goodness-of-fit	1.137	1.188	1.047	1.011	1.122
final R indices [$I > 2\sigma(I)$]	$R_{\text{obs}} = 0.0566$	$R_{\text{obs}} = 0.0408$	$R_{\text{obs}} = 0.0481$	$R_{\text{obs}} = 0.0551$	$R_{\text{obs}} = 0.0505$
R indices [all data]	$wR_{\text{obs}} = 0.1429$ $R_{\text{all}} = 0.0835$ $wR_{\text{all}} = 0.1636$	$wR_{\text{obs}} = 0.0982$ $R_{\text{all}} = 0.0516$ $wR_{\text{all}} = 0.1081$	$wR_{\text{obs}} = 0.1042$ $R_{\text{all}} = 0.0716$ $wR_{\text{all}} = 0.1155$	$wR_{\text{obs}} = 0.1026$ $R_{\text{all}} = 0.1065$ $wR_{\text{all}} = 0.1202$	$wR_{\text{obs}} = 0.1237$ $R_{\text{all}} = 0.0541$ $wR_{\text{all}} = 0.1269$
largest diff. peak and hole	0.904 and -0.547 e $\cdot\text{\AA}^{-3}$	1.776 and -1.280 e $\cdot\text{\AA}^{-3}$	2.157 and -1.240 e $\cdot\text{\AA}^{-3}$	1.934 and -1.818 e $\cdot\text{\AA}^{-3}$	1.909 and -2.158 e $\cdot\text{\AA}^{-3}$

^a $R = \sum ||F_o| - |F_c|| / \sum |F_o|$, $wR = \{ \sum [w(|F_o|^2 - |F_c|^2)^2] / \sum [w(|F_o|^4)] \}^{1/2}$ and $\text{calcd } w = 1 / [\sigma^2(F_o^2) + (0.0318P)^2 + 111.1197P]$, where $P = (F_o^2 + 2F_c^2) / 3$.

used pH as a tool for controlling the protonation and hence the extent of hydrolyzation of the diimide ligand. Thus, we can vary the crystallographic phase of the system with pH by in situ release of variable amounts of amino pyridine in the system. Controlled blank studies confirmed the mechanism of in situ hydrolysis of the ligand. Optical absorbance studies show that the hybrids have considerable band gap decrease from the constituent units (POM and 4-ap) resulting in the formation of semiconducting hybrids. The compounds have been characterized using single crystal X-ray diffraction (SCXRD), powder X-ray diffraction (PXRD), IR spectroscopy, and elemental analysis. Magnetic measurements showed that the compounds are diamagnetic, thereby confirming the hexavalent oxidation state of the molybdenum ions in the POM unit. In a proof-of-concept experiment, the selected compounds were tested for heterogeneous catalytic oxidation of small organic molecules, which showed that these hybrids are good heterogeneous catalysts for selective oxidation reactions.

2. EXPERIMENTAL SECTION

2.1. Reagents. All the chemicals were obtained from commercially available certified reagent sources and used without further purifications. Sodium molybdate dihydrate ($\text{Na}_2\text{MoO}_4 \cdot 2\text{H}_2\text{O}$, AR, 99%), sodium silicate pentahydrate ($\text{Na}_2\text{SiO}_3 \cdot 5\text{H}_2\text{O}$, LR, 97%), and cupric chloride dihydrate ($\text{CuCl}_2 \cdot 2\text{H}_2\text{O}$, AR, 99.9%) were obtained from Spectrochem. Concentrated HCl and acetone (GC, 95%) were purchased from Merck. Glacial acetic acid (CH_3COOH , 16 N, 99.99%) was purchased from Sigma-Aldrich. Millipore water of conductivity 18.2 M Ω -cm was used for synthesis and all other studies. NDI-pyridine was synthesized according to a reported procedure.²¹

2.2. Synthesis. The hybrid materials **1**: $[\text{H}_4(\text{SiMo}_{12}\text{O}_{40})][(\text{C}_5\text{H}_6\text{N}_2)_6]$, **2**: $([\text{H}_8(\text{SiMo}_{12}\text{O}_{40})_2][(\text{C}_5\text{H}_6\text{N}_2)_{10}] \cdot 7\text{H}_2\text{O})$, **3**: $[\text{H}_8(\text{Mo}_{12}\text{O}_{40}\text{Si})_2][(\text{C}_5\text{H}_6\text{N}_2)_9] \cdot 7(\text{H}_2\text{O})$, **4**: $[\text{H}_8(\text{Mo}_{12}\text{O}_{40}\text{Si})_2][(\text{C}_5\text{H}_6\text{N}_2)_7] \cdot 6(\text{H}_2\text{O})$, and **5**: $[\text{H}_8(\text{Mo}_{12}\text{O}_{40}\text{Si})_2][(\text{C}_5\text{H}_6\text{N}_2)_7] \cdot 7(\text{H}_2\text{O})$ were synthesized under hydrothermal conditions, using 50 mL Teflon lined autoclave chambers under autogenous pressure. The autoclaves were filled with 35 mL of distilled water (70% volume capacity), followed by the addition of 0.5 g (2.07 mmol) of $\text{Na}_2\text{MoO}_4 \cdot 2\text{H}_2\text{O}$ with stirring. Glacial acetic acid (16 N) was then added dropwise to adjust the pH of the solution between 4 and 5. To this solution, 0.5 g (2.36 mmol) of

$\text{Na}_2\text{SiO}_3 \cdot 5\text{H}_2\text{O}$ was added, followed by glacial acetic acid to maintain the pH between 4 and 5. Consequently, the initial transparent solution became yellowish green. In the next step, 0.238 g (1.4 mmol) of $\text{CuCl}_2 \cdot 2\text{H}_2\text{O}$ and 0.59 g (1.73 mmol) of NDI-py were added to obtain a greenish blue solution of pH around 4.6. In the final step, precise pH control was achieved by successive addition of concentrated and dilute HCl, very slowly to adjust the pH between 1 and 5, as required for different reactions. The reaction mixture was stirred for 1 h and was kept at 180 °C for 5 days.

The reactions were carried out at pH 1.2, 2.2, 3.2, 4.2, and 4.5 to understand the formation of different phases without varying the POM/4-ap ratio. The single crystals were obtained in good yields (55–65% w.r.t. $\text{Na}_2\text{MoO}_4 \cdot 2\text{H}_2\text{O}$, 1: 64%, 2: 62%, 3: 55%, 4: 59%, and 5: 58%) directly from the solution on cooling. They were separated and washed with distilled water and acetone.

2.3. Powder X-ray Diffraction (PXRD). Phase identity and purity of the compounds were checked by PXRD, which was done on a Bruker X8 Discover diffractometer using $\text{Cu K}\alpha$ radiation ($\lambda = 1.5418 \text{ \AA}$). Data were collected over the angular range $3^\circ \leq 2\theta \leq 50^\circ$, with a step size of 0.02° at room temperature calibrated against corundum standards. The comparison of experimental PXRD with the simulated single crystal XRD patterns of compounds 1–5 is shown in Figure S2.

2.4. Single Crystal X-ray Diffraction (SCXRD). Single crystals of the compounds 1–5 were mounted on a thin glass fiber with commercially available super glue. X-ray single crystal data of the compounds were collected on a Bruker D8 Venture diffractometer (Photon CMOS detector) equipped with a microfocus, 2.4 kW sealed tube X-ray source with graphite monochromatic $\text{Mo-K}\alpha$ radiation ($\lambda = 0.71073 \text{ \AA}$) operating at 50 kV and 1 mA, with ω scan mode. The program SAINT²² was used for integration of diffraction profiles, and absorption correction was done with the SADABS²³ program. The structures were solved by direct methods, followed by successive Fourier and difference Fourier syntheses. All the non-hydrogen atoms except a disordered 4-ap ring were refined anisotropically. Calculations were carried out using SHELXL 97,²⁴ SHELXS 97,²⁴ PLATON,²⁵ WinGX system ver. 1.80.05,²⁶ and Olex2.²⁷ The data collection and refinement parameters for the compounds are summarized in Table 1. Due to high disorder in the systems, some B level alerts were obtained in the checkcif of the compounds, particularly in the cases of 3–5. These errors mainly arose from disordered 4-ap rings and due to hydrogen placements on the disordered centers.

2.5. Fourier Transform Infrared Spectroscopy (FT-IR). FT-IR spectra were obtained for 1–5 on a Bruker IFS 66v/S instrument. The pellets were prepared with dried KBr, and the KBr spectrum was used as a reference. Clean single crystals of the respective compounds were used for measurements. The KBr–sample mixtures were used to make 13 mm diameter pellets for the measurements. The spectra were recorded in between 400 and 4000 cm^{-1} . The IR spectra for the compounds 1–5 are shown in Figure S8 (in the region of $4000\text{--}400 \text{ cm}^{-1}$). Various modes of IR stretching frequencies for all the compounds and their assignment have been tabulated in Table S1. The overall spectra of all the compounds are similar owing to the commonality of the chemical species present in the structures. The spectra for compounds 1–5 are a combination of stretching frequencies for the two units, POM and the 4-ap group. The stretching frequencies for the 4-ap group mainly fall above 1000 cm^{-1} (except for the bending modes), while those for the POM unit are observed below 1000 cm^{-1} .^{28–32} The broad O–H band at 3400 cm^{-1} , observed for the compounds 2–5, is due to the presence of the lattice water molecules which somewhat masks the N–H stretch expected in the same region. The N–H stretch in the case of compounds 1 and 2 is quite sharp at 3446 cm^{-1} . The other important stretching frequencies originating from the 4-ap groups in all the compounds are observed at $\sim 2900\text{--}3000 \text{ cm}^{-1}$, which are characteristic of C–H stretching (sym and asym) of the aromatic group. Other important peaks observed are aromatic C=C stretch at $\sim 1520 \text{ cm}^{-1}$, C=N stretch at $\sim 1650 \text{ cm}^{-1}$, N–H bending at $\sim 1587 \text{ cm}^{-1}$, and C–N at 1380 cm^{-1} . The slight shift in the positions of N–H, C–H, and C=C stretching frequencies is due to the extensive hydrogen bonding interactions present in all the structures. The peaks corresponding to the POM unit ($\text{SiMo}_{12}\text{O}_{40}$) are observed at $\sim 1045 \text{ cm}^{-1}$ (Mo–O_v), 940 cm^{-1} (Si–O_c),

886 cm^{-1} (Mo–O_b–Mo, corner shared), and 770 cm^{-1} (Mo–O_b–Mo, edge shared).^{29,30} Thus, the IR spectra clearly support the presence of 4-ap and the POM in all the compounds and confirm the crystal structures obtained from SCXRD.

2.6. UV–vis Spectroscopy. The compounds in powdered form were used for recording UV–vis spectra in reflectance mode on a PerkinElmer Lambda750 spectrophotometer. BaSO_4 was used as the reference for solid UV–vis absorbance spectroscopy. The samples were loaded in a solid sample holder with a transparent quartz window, and the measurements were performed in the range 200–800 nm. All obtained spectra were subtracted with the BaSO_4 spectrum as the background.

2.7. Scanning Electron Microscopy (SEM) and Elemental Analysis. Clean single crystals of the samples were loaded on a carbon tape, and the FESEM measurement was done on a Quanta3D (FEI) system, equipped with a monoCL4 cathodoluminescence system (GATAN). Data were collected with an accelerating voltage of 20 keV and a 50 s accumulation time. The EDAX measurements were performed on single crystals with a clean surface using a Bruker 129 eV EDAX instrument (Table S2) to check the presence of the elements for all 5 compounds. The EDAX analyses were performed using the P/B-ZAF standardless method (where P/B = peak-to-background model, Z = atomic no. correction factor, A = absorption correction factor, and F = fluorescence factor). EDAX of each sample was done over three different positions, and the overall composition was taken as the average of the three data sets. CHN analyses were carried out using a Thermo Scientific Flash 2000 CHN analyzer. The elemental percentages obtained from SCXRD data broadly matched with the elemental composition obtained from elemental analyses.

2.8. Nuclear Magnetic Resonance Spectroscopy (NMR). NMR was used to analyze the products of the reactions during the synthesis. NMR spectra were recorded with a Bruker AVANCE 400 (400 MHz) Fourier transform NMR spectrometer with chemical shifts reported in parts per million (ppm) with respect to TMS. Splitting patterns are designated as s, singlet; d, doublet; bs, broad singlet; m, multiplet; t, triplet. The samples (crystals/powders) were dissolved in chloroform-D solvent ($\delta = 7.26 \text{ ppm}$ for ^1H). Product of blank NDI-py (Figure S3a–c), ^1H NMR (400 MHz, CD_3OD , TMS): δ (ppm) 7.96 (d, 2H), 6.83 (d, 2H), crystals of blank NDI-py hydrolysis (Figure S3d), ^1H NMR (400 MHz, CD_3OD , TMS): δ (ppm) 7.63 (d, 4H).

2.9. Magnetic Measurement. Magnetic measurements on samples 1–3 were carried out on a Quantum Design MPMS-SQUID magnetometer. The compounds were powdered and screened by PXRD to confirm phase purity before doing magnetic measurements. Temperature dependent magnetic susceptibility data were collected for field-cooled (FC) and zero-field-cooled (ZFC) modes between 2 and 300 K with an applied field of 1000 Oe. *M* vs *H* data were collected at 2 and 300 K between -60 and $+60 \text{ kOe}$. Since the compounds showed very similar magnetic properties, magnetism was studied on the first three compounds, comprising those being used for catalytic studies to see the oxidation state of the metal centers.

2.10. Catalytic Studies. The catalytic studies were carried out on small organic molecules (ethyl benzene, cyclohexanol, anthracene, benzyl alcohol, and cyclooctene) using compounds 1 and 2 (5 mg). Reaction conditions for each reaction were obtained from various literature procedures^{33–35} and are shown in Scheme 2. The products were analyzed by drawing 1 mL aliquots after reaction completion, which was injected into a Shimadzu GCMS-QP 2010 Plus gas chromatography instrument (coupled with a mass analyzer) to know quantitative amounts of products formed. The percentage conversion and yields were determined on the basis of the concentration of starting materials remaining after the reactions. Compounds 1 and 2 were taken as the representative of this class of hybrids, and catalytic studies were done using these compounds as the systems are completely undisturbed. Experimental details on catalytic studies are given in the Supporting Information.

2.11. Adsorption Measurements. Adsorption isotherms of N_2 at 77 K were recorded with the dehydrated sample using a QUANTACHROME QUADRASORB-SI analyzer. About 50 mg of each of the samples 1, 3, and 5 were taken in a sample holder and

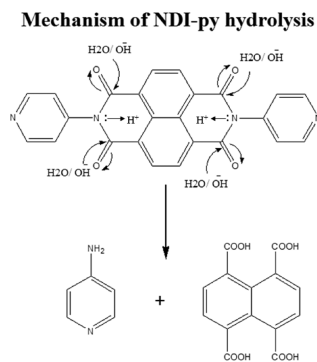
degassed at 100 °C under 10^{-1} Pa vacuum for about 12 h before the measurements to dehydrate the samples. Dead volume of the sample cell was measured using helium gas of 99.999% purity. Adsorbed gas amount was calculated from the pressure difference ($P_{\text{cal}} - P_e$), where P_{cal} is the calculated pressure with no gas adsorption and P_e is the observed equilibrium pressure. All the operations were computer-controlled and automatic. The BET surface areas of the compounds were found to be very low, as expected from the nonporous nature of the hybrids. The respective BET surface areas of the compounds 1, 3, and 5 were found to be 4.394, 2.842, and 2.298 m^2/g . The adsorption isotherms of the compounds are shown in Figure S10.

3.12. Thermogravimetric Analysis (TGA). The TGA analysis of compounds 1–5 was performed using a Mettler Toledo TGA 850 under a nitrogen atmosphere at a heating rate of 5 °C/min between 25 and 800 °C. The samples showed similar thermogravimetric behavior with sequential decays of lattice water molecules, followed by degradations of the organic ligands. The loss of water molecules (2–4%) mainly happened between 25 and 120 °C. The loss of organic ligands broadly occurred in two steps between 200 and 400 °C (~10%) and between 520 and 770 °C (20%). The TGA curves for 1–5 are provided in Figure S11.

3. RESULTS AND DISCUSSIONS

3.1. Synthesis and Crystal Growth. Phase modulation by the slow release of ligand and controlled protonation may be an innovative technique to engineer the crystal structure of POM-organic hybrids. However, such fine modulations are difficult in rigid indirect covalent POM hybrid systems as the secondary TMs bind the ligands into high dimensional rigid structures. Supramolecular structures on the other hand, are far less rigid and give wider windows for structural fine-tuning and consequent engineering of crystal phases. To have a better control on the overall reactivity of the ligand, here we have used the simple ligand, 4-ap pyridine, in the form of a hydrolyzable precursor, NDI-Py. NDI-py is well-known for its photophysical properties,²¹ having rich electronic properties and is known to be quite stable under acidic conditions.²¹ However, it failed to survive the harsh hydrothermal acidic reaction conditions and degraded (pH 1–4.5, 180 °C for 5 days) to yield 4-ap and naphthalene tetracarboxylic acid (Scheme 1). The dissociation leads to the in situ formation of crystals of hybrid compounds of POM (Keggin: $\text{SMo}_{12}\text{O}_{40}^{6-}$ and 4-ap). Neither solution phase synthesis at milder reaction conditions nor reactions at relatively lower temperature of 160 °C yielded any NDI-py incorporated systems. To check the effect of reaction conditions and chemical

Scheme 1. Schematic Representation of the Mechanism of NDI-py Hydrolysis^a



^aThe naphthalene tetracarboxylic acid might exist as the dianhydride as well which was confirmed from the NMR spectra and SCXRD analysis.

environment in the in situ hydrolysis of NDI-py, the following three controlled reactions were performed: (a) blank NDI-py reaction (without POM precursors), (b) the reaction of 4-ap with POM precursors, and (c) the reaction of NDI-py with POM precursors maintaining the same reaction conditions (temp: 180 °C, pH: 1–2, time: 5 days). The product solutions were analyzed through NMR (Figure S3) which shows that all the three reactions generated the same organic species in solution, i.e., 4-ap. NMR spectra of the product obtained from the three control reactions confirm the in situ generation of 4-ap or equivalent species through hydrolysis of NDI-py and show how the hydrolysis is affected by the chemical environment. The two solid compounds shown, orange color crystalline mass (Figure S3a, inset) and the red crystals (at the bottom, Figure S2d, left inset), were obtained in the blank NDI-py reaction. In the inset of Figure S3d, the optical image and solved structure of the red crystals are shown. The blank NDI-py reaction yielded two solid products (Figure S3, insets of (a) and (d)), both of which were also analyzed through NMR and SCXRD. The NMR of the orange color crystalline product (Figure S3a, inset) was found to be the same as the solution NMR spectra obtained for the three control reactions, signifying the in situ formation of 4-ap. The NMR data of the red crystals (Figure S3d, inset) showed that it is the other half of hydrolyzed NDI-py, i.e., naphthalene acid dianhydride, which was later reconfirmed from the SCXRD analysis (Figure S3d, right inset). This proves that NDI-py is indeed generating the 4-ap in situ and this hydrolysis is affected only by conditions like temperature, pressure, and pH of the reaction, and not by any chemical precursor.

The results of the controlled synthetic studies indicated the occurrence of an acid catalyzed hydrolysis of NDI-py, which prompted us to use pH as a tool to tune the extent of hydrolysis and modulate the phase of the resulting hybrids. Hydrothermal reactions were set at different pH conditions (1.2, 2.3, 3.2, 4.2, and 4.5), maintaining otherwise identical reaction conditions. Interestingly, we found pH to play a crucial role in the phase formation of the hybrid structures where the amount of 4-ap incorporation is changing with changing pH conditions, leading to the different crystal structures of the POM-amino pyridine hybrid. Compounds 1: $[\text{H}_4(\text{SiMo}_{12}\text{O}_{40})][(\text{C}_5\text{H}_6\text{N}_2)_6]$, 2: $[\text{H}_8(\text{SiMo}_{12}\text{O}_{40})_2][(\text{C}_5\text{H}_6\text{N}_2)_{10} \cdot 7\text{H}_2\text{O}]$, 3: $[\text{H}_8(\text{Mo}_{12}\text{O}_{40}\text{Si})_2][(\text{C}_5\text{H}_6\text{N}_2)_9 \cdot 7(\text{H}_2\text{O})]$, 4: $[\text{H}_8(\text{Mo}_{12}\text{O}_{40}\text{Si})_2][(\text{C}_5\text{H}_6\text{N}_2)_7 \cdot 6(\text{H}_2\text{O})]$, and 5: $[\text{H}_8(\text{Mo}_{12}\text{O}_{40}\text{Si})_2][(\text{C}_5\text{H}_6\text{N}_2)_7 \cdot 7(\text{H}_2\text{O})]$ were formed at pH 1.2 and 2.2, 3.2, 4.2, and 4.5, respectively. More POM hybrid crystal structures with varying 4-ap arrangements were obtained until pH 4.5, after which the formation of POM gets affected due to higher pH conditions. All the compounds (1–5) crystallized as dark blue colored crystals. SEM images of single crystals of the compounds 1–5 are shown in Figure S1. The crystals were found to be stable under normal conditions and in common laboratory solvents. These crystals were insoluble in water and common organic solvents. The controlled phase modulation study showed that pH plays an important role in the overall crystal phase formation of the hybrid by controlling the extent of hydrolyzation of the ligand NDI-pyridine. Alternatively, when we carried out the reactions with 4-ap directly, in the majority of the cases (75%), we have ended up with a mixture of different phases of POM-4-ap supramolecular hybrids.

3.2. Crystal Structure and pH Controlled Phase Modulation. Compound 1 synthesized at pH 1 crystallizes in a rhombohedral crystal system having $R\bar{3}$ space group with lattice parameters, $a = b = 21.8664(3)$ Å and $c = 10.5150(2)$ Å. The

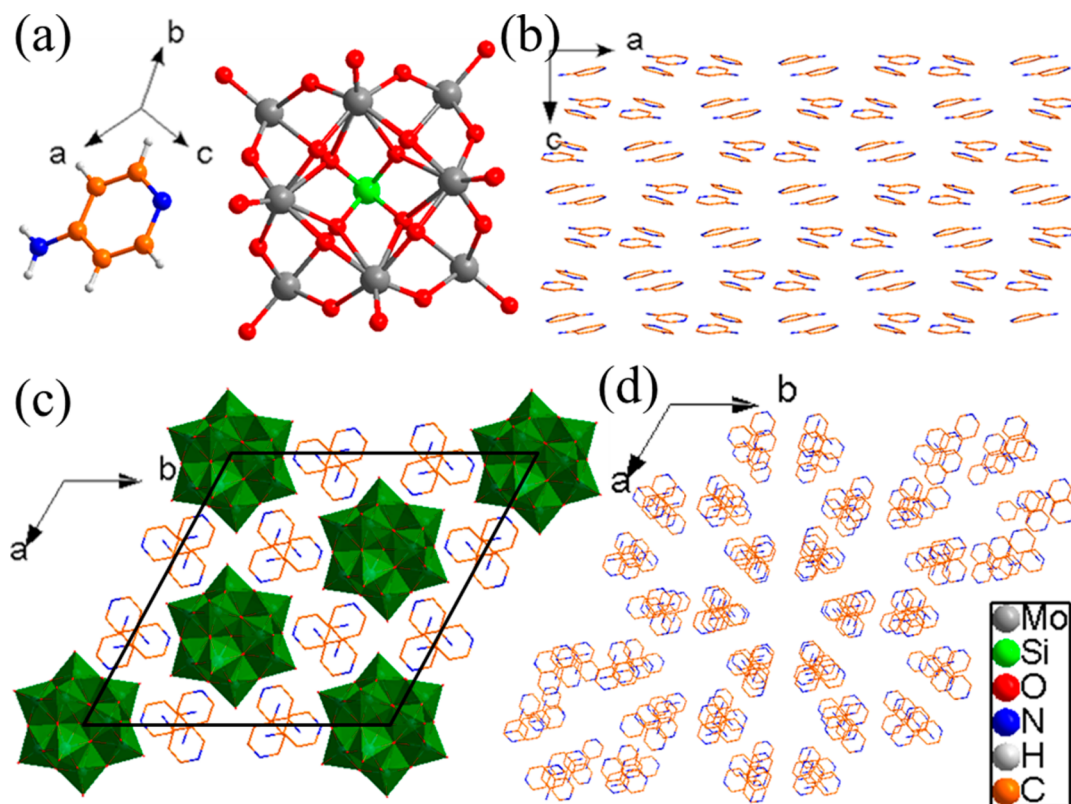


Figure 1. Crystal structure of the compound **1**: $[\text{H}_4(\text{SiMo}_{12}\text{O}_{40})][(\text{C}_5\text{H}_6\text{N}_2)_6]$. (a) Molecular structure, (b) arrangement of 4-ap molecules along the *b* direction, (c) unit cell, and (d) central projection of the ligand arrangement along the *c* direction.

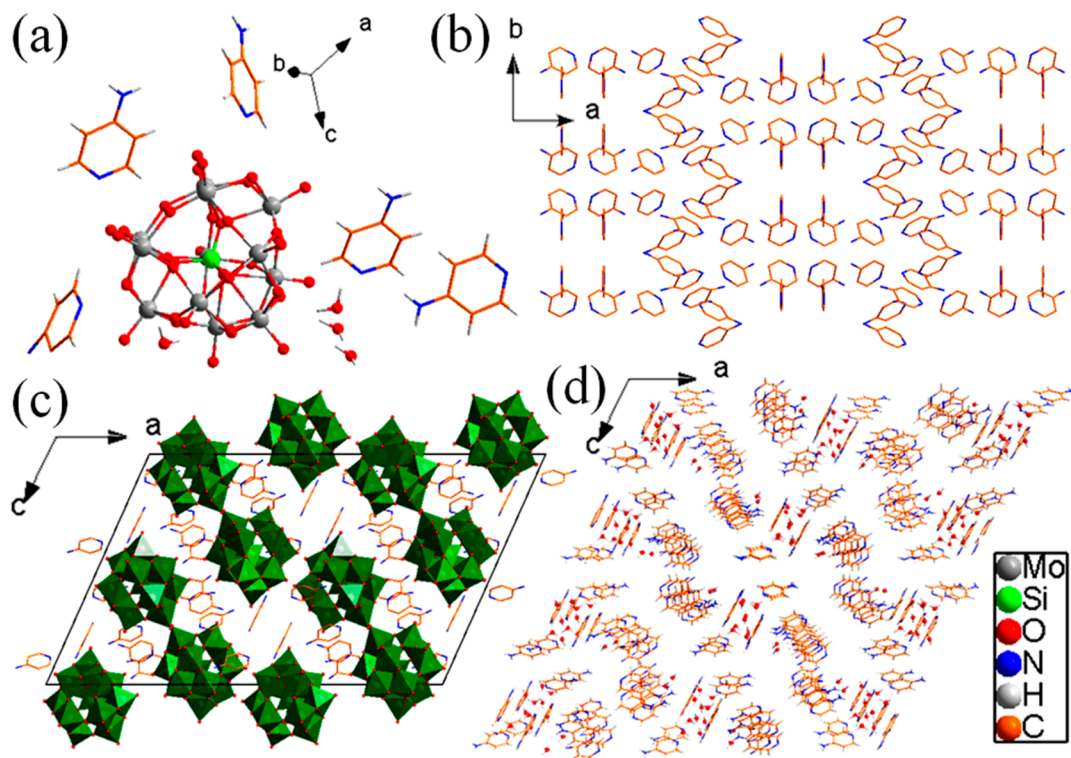


Figure 2. Crystal structure of the compound **2**: $[\text{H}_8(\text{SiMo}_{12}\text{O}_{40})_2][(\text{C}_5\text{H}_6\text{N}_2)_{10}] \cdot 7\text{H}_2\text{O}$. (a) Asymmetric unit, (b) arrangement of 4-ap molecules along the *c* direction, (c) unit cell, and (d) central projection of the ligand arrangement and lattice water molecules along the *b* direction.

structural arrangement in compound **1** is simpler as compared to the other hybrids of this family. The molecular structure of **1** (Figure 1a) consists of one POM unit and a 4-ap molecule

connected by supramolecular interactions. The asymmetric unit of **1** comprises one-third of a POM cluster and one 4-ap molecule. The molecular structure is generated through

symmetry operations, the formula unit of which has one POM unit and six 4-ap molecules. The unit cell structure and the 3D arrangement of the bipyridine rings are shown in Figures 1b–d and S4. The molecular structure of **1** is devoid of any lattice water molecules. The POM unit in **1** exists as disordered Keggin where the heteroatom Si is coordinated by eight half-occupied oxygen atoms. The 3D structure of **1** is formed mainly through supramolecular interactions like hydrogen bonding and C–H–O interactions. The amine groups and C–H of the 4-ap rings form hydrogen bonds with the terminal oxygen atoms of the POM unit. There is also parallel-displaced π – π stacking (4.2–4.4 Å) present among the 4-ap rings which adds further stability to the supramolecular hybrid structure.

Compound **2** was synthesized at pH 2.2. It crystallized in a monoclinic system with space group $C2/c$ having lattice parameters $a = 42.1438(2)$ Å, $b = 12.2492(5)$ Å, $c = 25.2517(10)$ Å, and $\beta = 115.802(3)^\circ$. The formula unit (Figure 2a) contains two such asymmetric units. Each one consists of one unit of the POM ($\text{SiMo}_{12}\text{O}_{40}$) and five 4-ap molecules with four lattice water molecules. The unit cell structure of **2** and the arrangement of 4-ap molecules in the hybrid compound are shown in Figure 2b–d and Figures S5 and S6. Some of the terminal and corner shared oxygen atoms of the POM unit form strong hydrogen bonds with the water molecules and the amine groups of 4-ap molecules. One of the 4-ap molecules (N10) is disordered at the amine position (N10 and N10A, Figure S5). The 2D and 3D hybrid structures are made up of supramolecular interactions like intermolecular hydrogen bonding, C–H–O interaction (C–H of 4-ap molecules and O of water or POM), π – π stacking, and electrostatic interactions. Moreover, there are moderately strong π – π interactions present between the aromatic 4-ap rings (π – π distance ~ 3.65 – 3.75 Å) which provide further stabilization to the 3D structure.

Compound **3**, synthesized at a pH of 3.2, crystallized in $P2_1/n$ space group with lattice parameters $a = 21.2231(13)$ Å, $b = 12.3452(7)$ Å, $c = 22.995(14)$ Å, and $\beta = 113.16(2)^\circ$. The formula unit shows the presence of two POM units, nine 4-ap moieties, and seven lattice water molecules. The molecular unit (Figure 3a) consists of half of the formula unit. The 3D supramolecular hybrid structures are formed through non-covalent interactions like H-bonding (b/w the 4-ap amine protons, lattice water hydrogen atoms, and terminal O atoms of the POM), C–H– π and π – π interactions between the 4-ap molecules, and CH–O interactions between the 4-ap and the lattice water molecules. The arrangement of the 4-ap units and lattice water molecules in the molecular structure is shown in Figure 4c. There are two strongly disordered 4-ap units in the structure of **3** (Figure 4c). The disorder in the two units was successfully resolved where, in one unit, there was a superimposition of two 180° rotated 4-ap rings, while, in the other, two laterally half-translated 4-ap moieties were superimposed (Figure S7a).

Compounds **4** and **5** were synthesized at pH of 4.2 and 4.5, respectively. Both compounds crystallized in the triclinic system of space group $P\bar{1}$ with the lattice parameters $a = 10.4802(7)$ Å, $b = 11.7748(8)$ Å, $c = 21.0804(15)$ Å, $\alpha = 75.265(4)^\circ$, $\beta = 77.340(3)^\circ$, $\gamma = 86.720(4)^\circ$ for compound **4** and $a = 11.3922(5)$ Å, $b = 15.1799(6)$ Å, $c = 15.9743(7)$ Å, $\alpha = 91.188(2)^\circ$, $\beta = 107.447(2)^\circ$, $\gamma = 100.744(2)^\circ$ for compound **5**. The molecular structures of compounds **4** and **5** are shown in Figure 3b,c. Owing to their similar synthesis conditions, both the compounds have a similar 4-ap-to-POM ratio of 3.5 in the formula unit. The difference between the two compounds lies in the number of

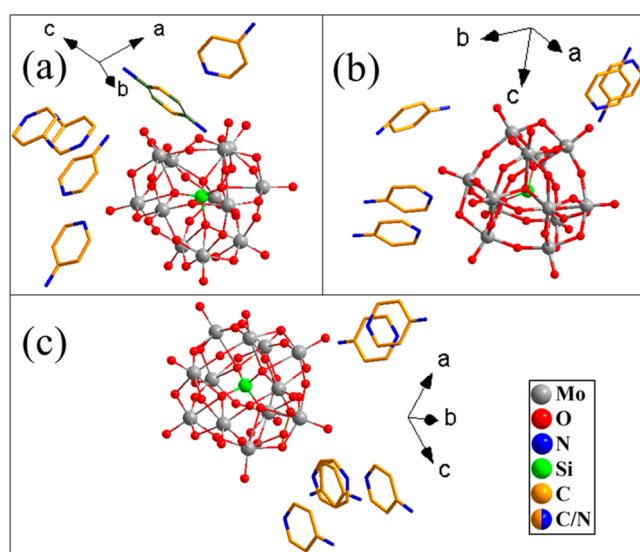


Figure 3. Molecular crystal structure of (a) **3**: $[\text{H}_8(\text{Mo}_{12}\text{O}_{40}\text{Si}_2)] \cdot [(\text{C}_5\text{H}_6\text{N}_2)_9] \cdot 7(\text{H}_2\text{O})$, (b) **4**: $[\text{H}_8(\text{Mo}_{12}\text{O}_{40}\text{Si}_2)] \cdot [(\text{C}_5\text{H}_6\text{N}_2)_7] \cdot 6(\text{H}_2\text{O})$, and (c) **5**: $[\text{H}_8(\text{Mo}_{12}\text{O}_{40}\text{Si}_2)] \cdot [(\text{C}_5\text{H}_6\text{N}_2)_7] \cdot 7(\text{H}_2\text{O})$. Hydrogen atoms and lattice water molecules are omitted.

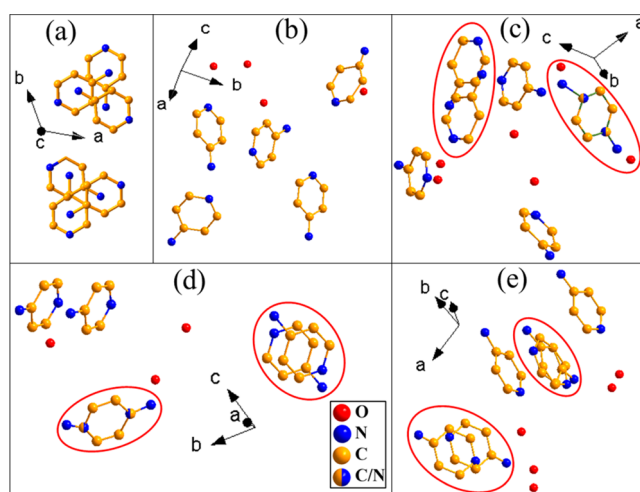


Figure 4. Arrangement of the 4-ap units and lattice water molecules in the molecular crystal structure of (a) **1**, (b) **2**, (c) **3**, (d) **4**, and (e) **5**. Hydrogen atoms are omitted for clarity. In the structure for compounds **3**, **4**, and **5**, the disordered 4-ap units are circled in red.

lattice water molecules (6 in compound **4** and 7 in compound **5**) and the molecular arrangements involving different supramolecular interactions as mentioned in the above structural descriptions. Both compounds had severe disorders in two 4-ap units. The kinds of disorder are different and have been pictorially resolved as shown in Figure S7b,c. In the case of **4**, both were two different kinds of 180° rotational disorders, while, in **5**, one disorder was pivotal $\sim 30^\circ$ rotation of the ring about one atom as the center.

pH dependent phase modulation study yielded many interesting observations which shine light on the mechanism of the crystal engineering in this class of supramolecular hybrids. As Figure 5 and molecular formula of the compounds **1**–**5** suggest, there is a clear role of pH in the extent of hydrolysis of the NDI-py molecule, thereby varying the amount of 4-ap available for the molecule formation. This occurs as the pH controls the protonation of the nitrogen center of the NDI-py unit, which

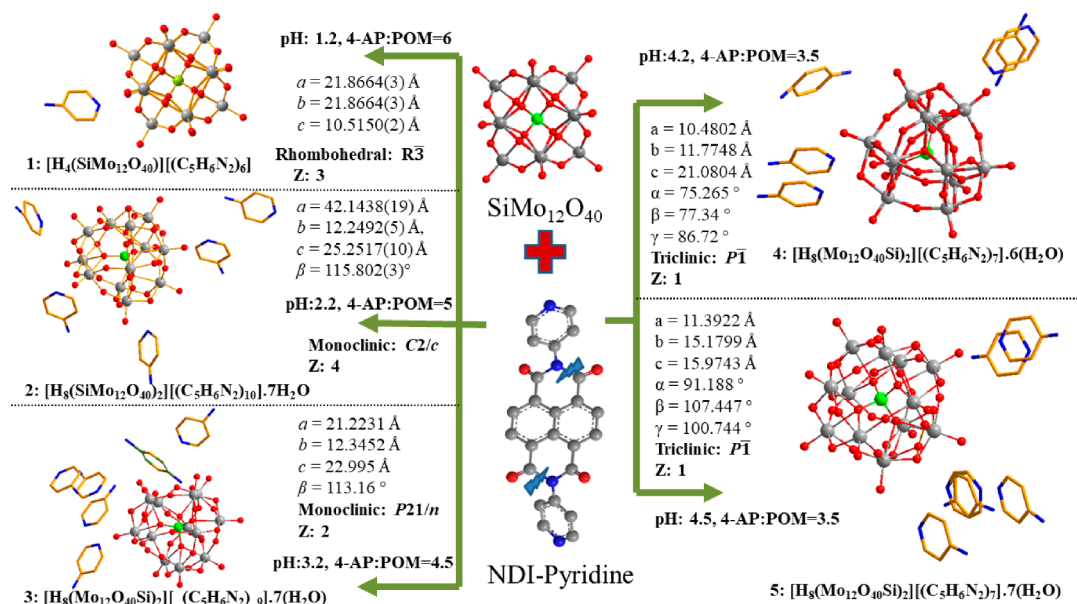


Figure 5. pH dependent controlled phase variation in the POM-AP hybrids. As we move from lower to higher pH, due to lower protonation and hydrolyzation of the NDI ligand, the AP-to-POM ratio is decreasing. However, with increase in pH, the hybrids are crystallizing with lesser symmetry.

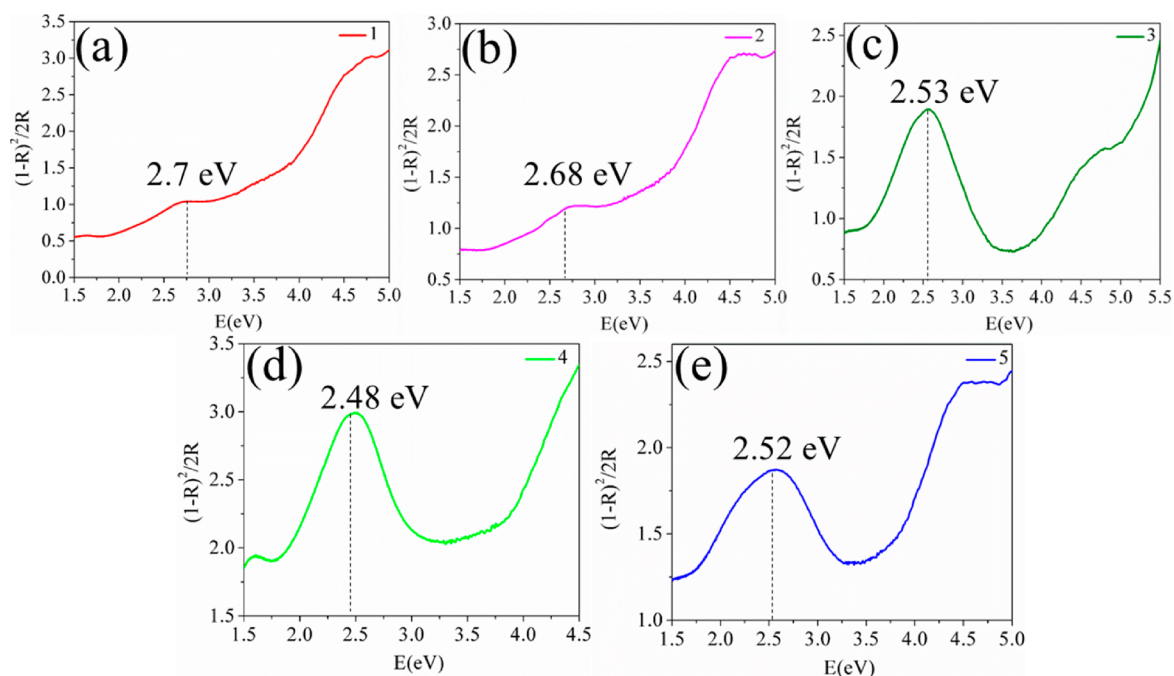


Figure 6. Kubelka–Munk plots of compounds 1–5. The band gaps were determined from the K-M plots of the DRS spectra of (a) 1: 2.7 eV, (b) 2: 2.68 eV, (c) 3: 2.53 eV, (d) 4: 2.48 eV, and (e) 5: 2.52 eV.

catalyzes its hydrolysis by water attack at the amide center (Scheme 1). This has also been proved by the blank controlled study of the NDI-py where we could identify the naphthalene anhydride through SCXRD along with the presence of 4-ap in the solution. It can be clearly observed that, as we move lower (1.2) to higher pH (4.5), the 4-ap-to-POM ratio also decreases almost linearly as 6 in compound 1, 5 in compound 2, 4.5 in compound 3, and 3.5 in compounds 4 and 5. From this observation, it is evident that lowering the H^+ concentrations decreases the extent of 4-ap formation, thereby lowering the 4-ap:POM ratio in the molecular crystal structure. Another interesting fact is the successive lowering in symmetry of the

system as we move from lower to higher pH, i.e., high to low 4-ap:POM ratio. Also, it is observed that, upon moving from compound 1 to 5, the extent of molecular disorder in the 4-ap units increases. This may be attributed to a lower concentration of 4-ap and a slower crystallization phenomenon.

3.3. UV–vis Spectroscopy and Band Gap. Electronic spectra of the solid powdered samples of 1–5 were recorded in reflectance mode in the range of 200–1000 nm (Figure S9). The two absorption bands observed at around 213 and 250 nm can be attributed to the LMCT and $n-\pi^*/\pi-\pi^*$ transitions of the ligand 4-ap, respectively.³⁶ The broad absorption band at ~335–360 nm can be assigned to the charge transfer transition in the

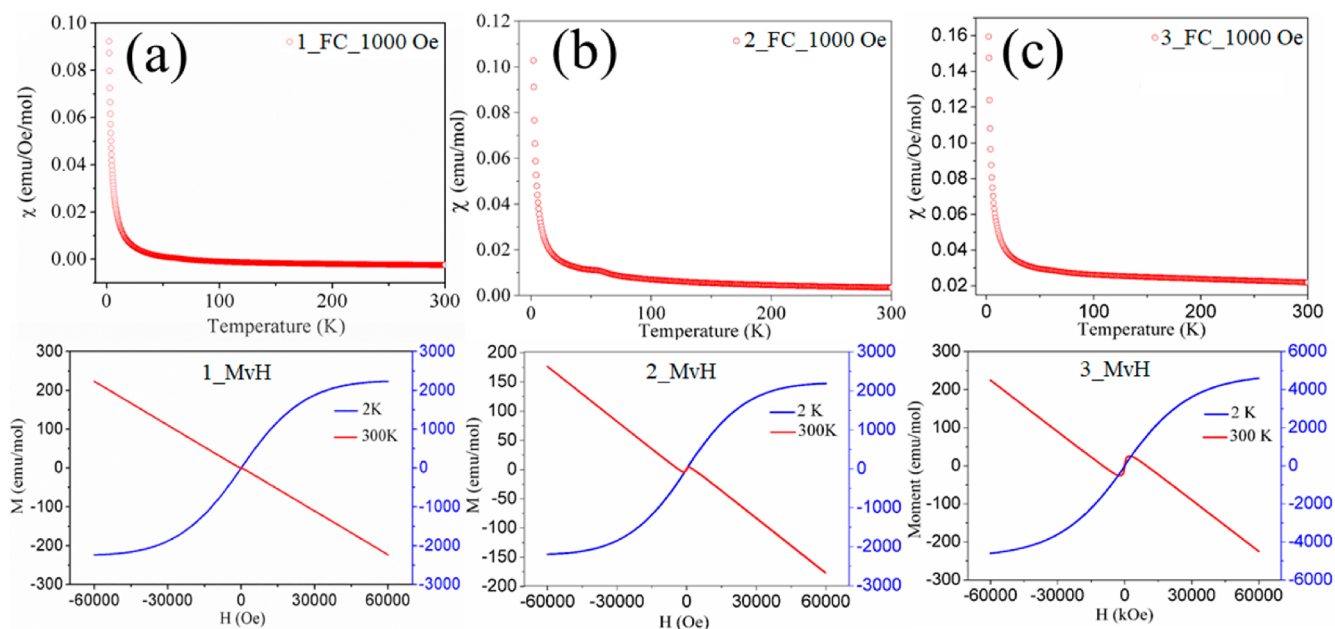


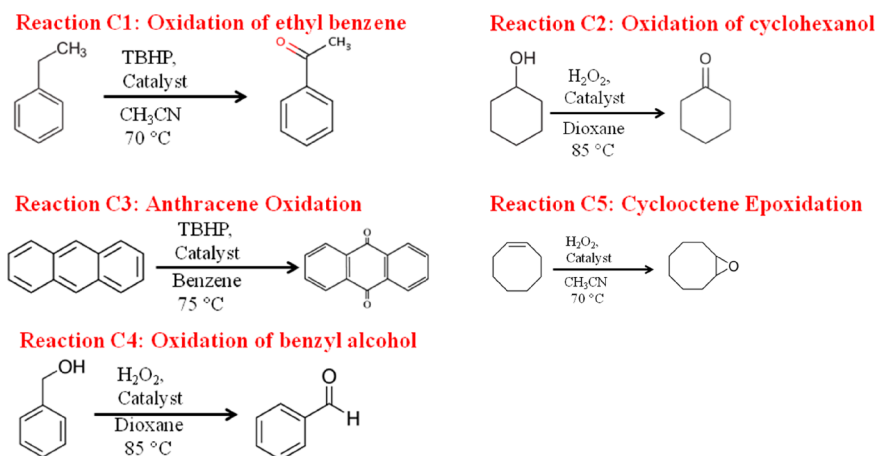
Figure 7. Temperature dependent magnetic susceptibility in FC mode (top) and field dependent magnetization (bottom) of the compounds **1** (a), **2** (b), and **3** (c).

compounds.³⁶ The DRS spectra were converted to a Kubelka–Munk (K-M) function plot^{32,37} (Figure 6), and the optical band gaps were determined as the energy value (in eV) for the first prominent peak maxima in the K-M plot. The optical band gap was determined to be 2.7, 2.68, 2.53, 2.48, and 2.52 eV for **1–5**, respectively, which falls in the semiconducting region. It is to be noted that the two comprising units of the hybrid structures, i.e., 4-ap and $\text{SiMo}_{12}\text{O}_{40}$, are known to exist as insulators.³² There is a clear transition from insulator to semiconductor state as we move from the individual units to the hybrid structure. This is probably occurring because of the enhanced band structure in the case of the hybrids than the individual molecules in the solid state.³⁸ Due to interactions between the POM and ligand units, new bands arise above and below the valence and conduction bands, which eventually leads to the decrease in band gap of the hybrids.

3.5. Magnetic Properties. Magnetic measurements were performed on powdered crystalline samples of compound **1–3** in the range 2–300 K at an applied magnetic field of 1000 Oe (field-cooled) to check the oxidation states of molybdenum atoms and to see the overall magnetic properties of the hybrid. It is expected that all the Mo ions are in their highest oxidation state (+6) and hence nonmagnetic, devoid of any d-electrons. The variation of molar magnetic susceptibility (χ_M) with temperature (T) for **1**, **2**, and **3** is depicted in Figure 7a–c, respectively. The plots clearly show that the compounds are diamagnetic in nature as the χ_M values are negative in the entire temperature range of 100–300 K. Below 70 K, there is an increase in magnetic susceptibility (small hump, more pronounced in Figure 7b,c), which may be originating from a small amount of paramagnetic γ oxygen impurity (arising from insufficient purging) present in the system which crystallizes at low temperatures. Paramagnetic solid γ oxygen is a paramagnetic phase with an A15 cubic structure.³⁹ Field dependent magnetic moment studies were done at 2 and 300 K (Figure 7a–c, bottom). The negative slope of field dependent magnetization data (M vs H) at 300 K clearly indicates that the systems are of diamagnetic nature at room temperature. This is expected as the systems are devoid of any unpaired electrons particularly on the Mo metal centers. On the

other hand, the field dependent magnetization data at 2 K represents a typical sigmoid curve which saturates at higher fields. The sigmoid curve confirms the presence of a small amount of paramagnetism. The paramagnetic contribution at 2 K can be attributed to the crystallized paramagnetic oxygen present in the system. The saturation might be coming from some oxygen vacancies present at the sites of the 8 half-occupied oxygen atoms around Si present at the core of the POM. The vacant positions may contain some residual electrons which might account for such sigmoid curves at low temperatures. Overall, from the χ vs T data and the M vs H data at 300 K, it is clear that the compounds are diamagnetic and all the Mo in the compounds are in their +6 oxidation state.

3.6. Catalytic Studies. POMs have emerged as excellent catalysts for various types of catalytic reactions like acid catalyzed reactions, selective oxidations, hydrogenation reactions, and also for industrial catalysis because of their acidic and redox facile nature.^{40–42} Out of these, selective oxidation of small molecules is of immense importance in the field of catalysis as the end products are highly useful both in pharmaceuticals and as starting materials for various kinds of molecules, which forms the basis of chemical industries. Selective oxidation of molecules is challenging for both physical and synthetic chemists since most catalytic transformations have many oxidized products out of which the desired ones, in most cases, are not the thermodynamic or kinetic end product. Thus, the need for controlling the reaction pathways to get the desired products, arresting the reactions from further oxidations, demands the use of suitable catalysts. POMs have catered to this catalytic need for a long time. However, the major drawback while using POMs in catalysis is their high solubility in aqueous and polar organic solvents.⁴³ Due to their solubility and homogeneous mode of activity, recovering the catalyzed products and their application in practical devices is hampered. Though the homogeneous catalytic activities of POMs are very well studied and usually higher than that of heterogeneous cases, for practical applications, heterogeneous catalysis is more desirable. To overcome this issue, various methods have been adopted for the

Scheme 2. Scheme of the Various Organic Catalysis Reactions^a

^aHere, we studied the selective oxidations of small organic molecules by the catalysts. The amount of catalyst used in each reaction was 5 mg.

Table 2. Catalytic Conversion and Selectivity of the Expected Products for the Oxidation of Various Small Organic Molecules^a

code	reaction name	constituents		conditions	conversion (%)			selectivity (%)		
		reagents	amount		blank	1	2	blank	1	2
C1	oxidation of ethyl benzene	ethyl benzene	0.3 mL (2.4 mmol)	12 h, 70 °C	30	65	60	45	acetophenone (100)	acetophenone (85)
		acetonitrile	8 mL							
		70% TBHP	0.745 mL (4.8 mmol)							
C2	oxidation of cyclohexanol	cyclohexanol	0.1 g	8 h, 85 °C	negligible	inactive	inactive			
		30% H ₂ O ₂	0.17 g							
		dioxane	5 mL							
C3	oxidation of anthracene	anthracene	0.05 g	12 h, 75 °C	20	40.5	49.3	50	anthraquinone (100)	anthraquinone (70)
		70% TBHP	0.125 g							
		benzene	5 mL							
C4	oxidation of benzyl alcohol	benzyl alcohol	0.108 g (1 mmol)	8 h, 85 °C	34	67.79	40	52	benzaldehyde (53)	benzaldehyde (100)
		30% H ₂ O ₂	0.17 g (5 mmol)							
		1,4-dioxane	5 mL							
C5	epoxidation of cyclooctene	cyclooctene	1 g (10 mmol)	10 h, 85 °C	negligible	65.3	20		cyclooctene epoxide (41)	cyclooctene epoxide (32)
		TBHP	0.136 g (4 mmol)							
		1,4-dioxane	10 mL							

^a5 mg catalyst.

immobilization of POMs involving processes like forming POM hybrids with organic ligands, use of ionic liquids, loading POMs onto metal organic frameworks/mesoporous materials, and use of water insoluble salts of POMs (e.g., Cs⁺).^{40,43,44}

Here, we chose selective oxidation of small organic molecules to check catalytic property of the hybrids. A set of five peroxide based catalysis reactions, (1) oxidation of ethyl benzene, (2) oxidation of cyclohexanol, (3) oxidation of anthracene, (4) oxidation of benzyl alcohol, and (5) epoxidation of cyclooctene, were screened to study the oxidative properties of these hybrids. All catalytic studies were performed using pure powdered samples of compounds 1 and 2 as the catalyst. These compounds were chosen as the representative of this class of hybrids for catalytic studies as these were systems without disorders. The products of the catalysis reactions were analyzed through gas chromatography. The products, percentage conversions, and selectivity of the catalysis reactions by 1, 2 and the blank

reactions are given in Scheme 2, Table 2, and Figure 8. Comparing the blank and catalyzed reactions, we found that both

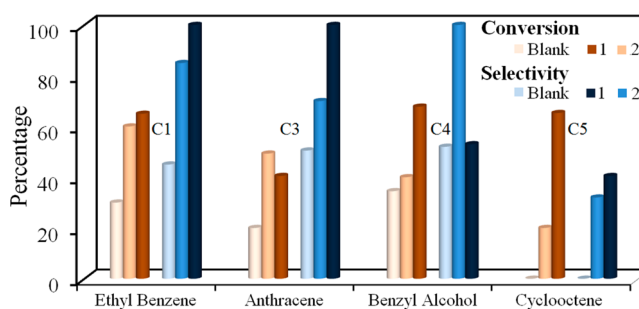


Figure 8. Comparison of the percentage conversion and selectivity of blank and catalyzed (compounds 1 and 2) oxidation of small organic molecules.

Table 3. Comparison of Catalytic Activity of Similar POM Based Systems for Small Molecule Oxidation

catalysis	catalyst	conversion (%)	selectivity/yield (%)	ref
alkylation of 2-methylnaphthalene	isopolytungstate supported on zirconia	>92	>95%	46
isobutyraldehyde oxidation	TBA ₄ HPW ₁₁ CoO ₃₉	94	54	42
	TBA ₃ PW ₁₁ CoO ₃₉	71	40	
	Na ₃ PW ₁₁ CoO ₃₉			
formaldehyde oxidation	TBA ₄ HPW ₁₁ CoO ₃₉	20	5	
	TBA ₃ PW ₁₁ CoO ₃₉	12	3	
	Na ₃ PW ₁₁ CoO ₃₉	19	9	
liquid-phase oxidation of anthracene	H ₅ [PMo ₁₀ V ₂ O ₄₀].32.5H ₂ O, supported on SBA-15	60	100	34
benzyl alcohol oxidation	H ₅ [PMo ₁₀ V ₂ O ₄₀].32.5H ₂ O, + SBA-15 + [C ₄ mim] ⁺		98	47
cyclohexanol oxidation			99	
cyclooctene oxidation	ZrO ₂ and Keggin-type 12-phosphomolybdic acid	82	100	35
cyclohexene oxidation		30	47	
styrene oxidation		30	5	
ethyl benzene oxidation	{[Cu ₂ (4,4-bipy) ₄ (H ₂ O) ₄](SiW ₁₂ O ₄₀)(H ₂ O) ₁₈ } _n	56.8	88.1	33
oxidation of ethyl benzene	catalyst 1	65	100	this report
oxidation of cyclohexanol		inactive		
oxidation of anthracene		40.5	100	
oxidation of benzyl alcohol		67.79	53	
epoxidation of cyclooctene		65.3	41	

the compounds are active for the selective oxidation of small organic molecules. Catalysts **1** and **2** could successfully catalyze all the reactions except oxidation of cyclohexanol. Compound **1** showed excellent catalytic activity for the oxidation of ethyl benzene and anthracene with 100% selectivity toward the formation of the respective desired products of acetophenone and anthraquinone (Table 2, Figure 8). The percentage conversions were also much higher (~65% and 40%, respectively) in these two reactions compared to the blank reactions (~30% and 20%, respectively). For the other two reactions, i.e., oxidation of benzyl alcohol and epoxidation of cyclooctene, the catalyzed reactions showed higher conversions (2 times) than the blank reactions, but selectivity of the specific products was similar to that of the uncatalyzed reactions. Compound **2**, on the other hand, showed excellent selectivity for oxidation of benzyl alcohol (100%). Broadly, the catalytic activity of compound **1** was found to be better than that of compound **2**. Thus, as we move from uncatalyzed to catalyzed reactions, the selectivity for the desired products was greatly enhanced, inferring that both the compounds are good catalysts for the selective oxidation of small organic molecules. A comparison of the catalytic activity of catalyst **1** with similar reported catalysts for heterogeneous catalysis of small molecule oxidation has been presented in Table 3. It is well-known that homogeneous catalysis of selective oxidation by POMs in the presence of peroxides proceeds through the formation of the active catalytic species like the Ishii–Venturello complex,⁴¹ where the peroxide reacts with the POM cluster before oxygen transfer to the substrates. However, reaction mechanism in the case of heterogeneous catalysis by POM is less understood and may vary from system to system.⁴⁵ There are two processes which need to be understood in order to analyze the overall mechanism of the selective oxidation, i.e., the mechanism of substrate activation and the generation of active oxygen species. POMs, being redox active species, accept/donate electrons through the various steps of catalysis to activate the peroxide, which is the oxygen donating species. The integrated structure of the POM-hybrid complex will determine the pathways, kinetics, and extent of substrate oxidation in this case. Here, though we expect some interactions between the peroxide species and the POM of the

hybrid, the structure or nature of the active oxygen species is not completely understood. The marginally higher activity of **1** over **2** may be due to the different extent of selective substrate activations by the respective catalysts due to their different crystallographic structures. However, a complete understanding of the entire reaction mechanism needs further in-depth studies. The recyclability and stability studies were carried out over three cycles after washing the filtered catalyst each time before reuse. The recyclability test showed that the catalyst is quite stable and there was negligible drop in catalytic activity (3–5%) after three cycles. This slight decrease in catalytic activity can be attributed to the poisoning of the catalyst by the organic molecules present/formed in the solution.

4. CONCLUSION

Five different POM based supramolecular 3D hybrid compounds with varying crystallographic phases were synthesized using a hydrolyzable ligand under hydrothermal conditions of different pH. Mechanistic study on the degradation of the starting ligand proved that only the reaction conditions and not the in situ generated POM species are responsible for the hydrolysis of the ligand. pH dependent synthetic study yielded crystallographic phase modulation in the system. The mechanism of phase variation and role of pH were studied to find that varying pH conditions led to variation in the extent of protonation and hydrolyzation of the ligand, yielding different phases. Such controlled phase modulation studies will find many applications in crystal engineering. Crystal structure analysis revealed that the hybrid structures have been stabilized in three dimensions through supramolecular interactions like H-bonding, C–H–O interactions, and π – π stacking. The optical absorption studies showed that the hybrids formed are semiconducting in nature. Catalytic studies were done for small organic molecule oxidation with the catalysts. Selected compounds showed good catalytic activity and excellent selectivity for some of the desired products with **1** being slightly better than **2**. In this work, we have demonstrated a simple way of immobilizing POM by forming supramolecular hybrids with organic ligands, which can be used as good heterogeneous catalysts for oxidation reactions.

ASSOCIATED CONTENT

Supporting Information

The Supporting Information is available free of charge on the ACS Publications website at DOI: 10.1021/acs.inorgchem.7b02385.

The assignments of peaks in IR, figures of structural coordination environments of 1–5, IR spectra and comparison of simulated/experimental PXRD patterns of compounds 1–5, absorbance spectra of 1–5 (PDF)

Accession Codes

CCDC 1434040, 1434041, and 1565781–1565783 contain the supplementary crystallographic data for this paper. These data can be obtained free of charge via www.ccdc.cam.ac.uk/data_request/cif, or by emailing data_request@ccdc.cam.ac.uk, or by contacting The Cambridge Crystallographic Data Centre, 12 Union Road, Cambridge CB2 1EZ, UK; fax: +44 1223 336033.

AUTHOR INFORMATION

Corresponding Author

*Phone: 080-22082998. Fax: 080-22082627. E-mail: sebastiancp@jncasr.ac.in.

ORCID

Dundappa Mumbaraddi: 0000-0003-3099-9348

Subi J. George: 0000-0003-4429-5237

Sebastian C. Peter: 0000-0002-5211-446X

Notes

The authors declare no competing financial interest.

ACKNOWLEDGMENTS

We thank the Jawaharlal Nehru Centre for Advanced Scientific Research, Sheikh Saqr Laboratory, and Department of Science and Technology (DST), India, for financial support. S.R. thanks the University Grants Commission, India, for the research fellowship, and D.M. thanks UGC-DAE CSR, Mumbai Centre, for the project fellowship. The authors thank Mr. Abhijit Sen for magnetic measurements and Prof. Tapas K. Maji and Mr. Subhajit Laha for the BET surface area measurements. S.R. thanks Dr. Arpan Hazra for fruitful discussions regarding SC data analysis. S.C.P. acknowledges support from DST (Grant SB/FT/CS-07/2011). We are grateful to Prof. C. N. R. Rao for his constant support and encouragement.

REFERENCES

- (1) Dolbecq, A.; Dumas, E.; Mayer, C. R.; Mialane, P. Hybrid Organic–Inorganic Polyoxometalate Compounds: From Structural Diversity to Applications. *Chem. Rev.* **2010**, *110*, 6009–6048.
- (2) Proust, A.; Matt, B.; Villanneau, R.; Guillemot, G.; Gouzerh, P.; Izzet, G. Functionalization and post-functionalization: a step towards polyoxometalate-based materials. *Chem. Soc. Rev.* **2012**, *41*, 7605–7622.
- (3) Song, Y. F.; Tsunashima, R. Recent advances on polyoxometalate-based molecular and composite materials. *Chem. Soc. Rev.* **2012**, *41*, 7384–7402.
- (4) Katsoulis, D. E. A survey of applications of polyoxometalates. *Chem. Rev.* **1998**, *98*, 359–387.
- (5) He, J. Z.; Pang, H.; Wang, W. Q.; Zhang, Y.; Yan, B.; Li, X. R.; Li, S. J.; Chen, J. Uniform $M_3PM_{12}O_{40}$ center dot nH_2O ($M = NH_4^+$, K^+ , Cs^+) rhombic dodecahedral nanocrystals for effective antibacterial agents. *Dalton Trans.* **2013**, *42*, 15637–15644.
- (6) Li, X. R.; Xue, H. G.; Pang, H. Facile synthesis and shape evolution of well-defined phosphotungstic acid potassium nanocrystals as a highly efficient visible-light-driven photocatalyst. *Nanoscale* **2017**, *9*, 216–222.
- (7) Long, D. L.; Tsunashima, R.; Cronin, L. Polyoxometalates: Building Blocks for Functional Nanoscale Systems. *Angew. Chem., Int. Ed.* **2010**, *49*, 1736–1758.
- (8) Wang, Y. F.; Weinstock, I. A. Polyoxometalate-decorated nanoparticles. *Chem. Soc. Rev.* **2012**, *41*, 7479–7496.
- (9) Yvon, C.; Surman, A. J.; Hutin, M.; Alex, J.; Smith, B. O.; Long, D. L.; Cronin, L. Polyoxometalate Clusters Integrated into Peptide Chains and as Inorganic Amino Acids: Solution- and Solid-Phase Approaches. *Angew. Chem., Int. Ed.* **2014**, *53*, 3336–3341.
- (10) Khenkin, A. M.; Efremenko, I.; Martin, J. M. L.; Neumann, R. Polyoxometalate-Catalyzed Insertion of Oxygen from O₂ into Tin-Alkyl Bonds. *J. Am. Chem. Soc.* **2013**, *135*, 19304–19310.
- (11) Evangelisti, F.; Guttinger, R.; More, R.; Luber, S.; Patzke, G. R. Closer to Photosystem II: A Co₄O₄ Cubane Catalyst with Flexible Ligand Architecture. *J. Am. Chem. Soc.* **2013**, *135*, 18734–18737.
- (12) Sadakane, M.; Steckhan, E. Electrochemical properties of polyoxometalates as electrocatalysts. *Chem. Rev.* **1998**, *98*, 219–237.
- (13) Xu, B. B.; Xu, L.; Gao, G. G.; Yang, Y. B.; Guo, W. H.; Liu, S. P.; Sun, Z. Z. Multicolor electrochromic and pH-sensitive nanocomposite thin film based on polyoxometalates and polyviologen. *Electrochim. Acta* **2009**, *54*, 2246–2252.
- (14) Liu, S. Q.; Kurth, D. G.; Volkmer, D. Polyoxometalates as pH-sensitive probes in self-assembled multilayers. *Chem. Commun.* **2002**, *9*, 976–977.
- (15) Chi, Y. N.; Cui, F. Y.; Jia, A. R.; Ma, X. Y.; Hu, C. W. pH-Dependent syntheses of copper-quinoxaline-polyoxotungstate hybrids: variable role of Keggin-type polyanion in different pH conditions. *CrystEngComm* **2012**, *14*, 3183–3188.
- (16) Yang, L.; Hou, L. L.; Ma, P. T.; Niu, J. Y. pH-dependent assembly of saturated to dilacunary Keggin-based silicotungstate: [Cu(en)₂(H₂O)]₂[H₂en]{-SiW₁₀O₃₆[Cu(en)₂(H₂O)]₂}center dot 7.5H₂O. *J. Coord. Chem.* **2013**, *66*, 1330–1339.
- (17) Filippov, A. P.; Kovalenko, A. S.; Il'in, V. G. Formation of nanoperiodic structures based on keggins and lacunary anions of phosphotungstic acid and cationic surfactants. *Theor. Exp. Chem.* **1998**, *34*, 229–234.
- (18) Yu, F.; Kong, X. J.; Zheng, Y. Y.; Ren, Y. P.; Long, L. S.; Huang, R. B.; Zheng, L. S. pH-dependent assembly of 0D to 3D Keggin-based coordination polymers: Structures and catalytic properties. *Dalton T* **2009**, 9503–9509.
- (19) Zheng, P. Q.; Ren, Y. P.; Long, L. S.; Huang, R. B.; Zheng, L. S. pH-dependent assembly of Keggin-based supramolecular architecture. *Inorg. Chem.* **2005**, *44*, 1190–1192.
- (20) Chen, Z. Y.; Lu, J. H.; Yu, K.; Zhang, H.; Wang, L.; Wang, C. M.; Zhou, B. B. Nonclassical Phosphomolybdates with Different Degrees of Reduction: Syntheses and Structural and Photo/Electrocatalytic Properties. *Inorg. Chem.* **2016**, *55*, 8309–8320.
- (21) Guha, S.; Saha, S. Fluoride Ion Sensing by an Anion-pi Interaction. *J. Am. Chem. Soc.* **2010**, *132*, 17674–17677.
- (22) SAINT 6.02; Bruker AXS Inc.: Madison, WI, 2000.
- (23) Sheldrick, G. M. SADABS: Empirical Absorption Correction Program; University of Göttingen: Göttingen, Germany, 1997.
- (24) Sheldrick, G. M.; Schneider, T. R. SHELXL: High-resolution refinement. *Methods Enzymol.* **1997**, *277*, 319–343.
- (25) Spek, A. L. Single-crystal structure validation with the program PLATON. *J. Appl. Crystallogr.* **2003**, *36*, 7–13.
- (26) Farrugia, L. J. *J. Appl. Crystallogr.* **1999**, *32*, 837–838.
- (27) Dolomanov, O. V.; Bourhis, L. J.; Gildea, R. J.; Howard, J. A. K.; Puschmann, H. OLEX2: a complete structure solution, refinement and analysis program. *J. Appl. Crystallogr.* **2009**, *42*, 339–341.
- (28) Deng, Q.; Huang, Y. L.; Peng, Z. S.; Dai, Z. J.; Lin, M. R.; Cai, T. J. Crystal structure and catalytic properties of three inorganic-organic hybrid constructed from heteropolymolybdate and aminopyridine. *J. Solid State Chem.* **2013**, *200*, 60–69.
- (29) Rocchiccioli-Deltcheff, C.; Fournier, M.; Franck, R.; Thouvenot, R. Vibrational Investigations of Polyoxometalates. 2. Evidence for Anion-Anion Interactions in Molybdenum(VI) and Tungsten(VI) Compounds Related to the Keggin Structure. *Inorg. Chem.* **1983**, *22*, 207–216.

- (30) Bridgeman, A. J. Density functional study of the vibrational frequencies of alpha-Keggin heteropolyanions. *Chem. Phys.* **2003**, *287*, 55–69.
- (31) Dieterle, M.; Weinberg, G.; Mestl, G. Raman spectroscopy of molybdenum oxides - Part I. Structural characterization of oxygen defects in MoO_{3-x} by DR UV/VIS, Raman spectroscopy and X-ray diffraction. *Phys. Chem. Chem. Phys.* **2002**, *4*, 812–821.
- (32) Iyer, A. K.; Peter, S. C. Two-Dimensional Bicapped Supramolecular Hybrid Semiconductor Material Constructed from the Insulators alpha-Keggin Polyoxomolybdate and 4,4'-Bipyridine. *Inorg. Chem.* **2014**, *53*, 653–660.
- (33) Yu, F.; Zheng, P. Q.; Long, Y. X.; Ren, Y. P.; Kong, X. J.; Long, L. S.; Yuan, Y. Z.; Huang, R. B.; Zheng, L. S. Polyoxometalate-Based Metal-Organic Frameworks as Heterogeneous Catalysts for Selective Oxidation of Ethylbenzene. *Eur. J. Inorg. Chem.* **2010**, *2010*, 4526–4531.
- (34) Bordoloi, A.; Lefebvre, E.; Halligudi, S. B. Selective oxidation of anthracene using inorganic-organic hybrid materials based on molybdovanadophosphoric acids. *J. Catal.* **2007**, *247*, 166–175.
- (35) Armatas, G. S.; Bilis, G.; Louloudi, M. Highly ordered mesoporous zirconia-polyoxometalate nanocomposite materials for catalytic oxidation of alkenes. *J. Mater. Chem.* **2011**, *21*, 2997–3005.
- (36) Bu, Y.; Liu, R.; Zhen, M.; Li, F.; Sun, Z.; Xu, L. A hybrid compound containing polyoxoanions and organic dye cations with visible-light photocatalytic H₂ evolution activity. *Inorg. Chem. Commun.* **2015**, *62*, 34–36.
- (37) Kortun, G. *Reflectance Spectroscopy*; Springer-Verlag: New York, 1969.
- (38) Roy, S.; Sarkar, S.; Pan, J.; Waghmare, U. V.; Dhanya, R.; Narayana, C.; Peter, S. C. Crystal Structure and Band Gap Engineering in Polyoxometalate-Based Inorganic-Organic Hybrids. *Inorg. Chem.* **2016**, *55*, 3364–3377.
- (39) Nomura, T.; Matsuda, Y. H.; Takeyama, S.; Matsuo, A.; Kindo, K.; Her, J. L.; Kobayashi, T. C. Novel Phase of Solid Oxygen Induced by Ultrahigh Magnetic Fields. *Phys. Rev. Lett.* **2014**, *112*, 247201.
- (40) Kholdeeva, O. A.; Maksimchuk, N. V.; Maksimov, G. M. Polyoxometalate-based heterogeneous catalysts for liquid phase selective oxidations Comparison of different strategies. *Catal. Today* **2010**, *157*, 107–113.
- (41) Kozhevnikov, I. *Catalysts for Fine Chemical Synthesis: Catalysis by Polyoxometalates*; Wiley: Chichester, U.K., 2002; Vol. 2, p 220.
- (42) Kholdeeva, O. A.; Vanina, M. P.; Timofeeva, M. N.; Maksimovskaya, R. I.; Trubitsina, T. A.; Melgunov, M. S.; Burgina, E. B.; Mrowiec-Bialon, J.; Jarzebski, A. B.; Hill, C. L. Co-containing polyoxometalate-based heterogeneous catalysts for the selective aerobic oxidation of aldehydes under ambient conditions. *J. Catal.* **2004**, *226*, 363–371.
- (43) Zhou, Y.; Chen, G. J.; Long, Z. Y.; Wang, J. Recent advances in polyoxometalate-based heterogeneous catalytic materials for liquid-phase organic transformations. *RSC Adv.* **2014**, *4*, 42092–42113.
- (44) Vasylyev, M. V.; Neumann, R. New heterogeneous polyoxometalate based mesoporous catalysts for hydrogen peroxide mediated oxidation reactions. *J. Am. Chem. Soc.* **2004**, *126*, 884–890.
- (45) Hill, C. L. Progress and challenges in polyoxometalate-based catalysis and catalytic materials chemistry. *J. Mol. Catal. A: Chem.* **2007**, *262*, 2–6.
- (46) Lucas, N.; Bordoloi, A.; Amrute, A. P.; Kasinathan, P.; Vinu, A.; Bohringer, W.; Fletcher, J. C. Q.; Halligudi, S. B. A comparative study on liquid phase alkylation of 2-methylnaphthalene with long chain olefins using different solid acid catalysts. *Appl. Catal., A* **2009**, *352*, 74–80.
- (47) Bordoloi, A.; Sahoo, S.; Lefebvre, F.; Halligudi, S. B. Heteropoly acid-based supported ionic liquid-phase catalyst for the selective oxidation of alcohols. *J. Catal.* **2008**, *259*, 232–239.